Structure enhancement diffusion and contour extraction for electron tomography of mitochondria

Carlos Bazan, Michelle Miller and Peter Blomgren

July 19, 2008

Computational Science &
Engineering Faculty and Students
Research Articles

Database Powered by the
Computational Science Research Center
Computing Group & Visualization Lab

COMPUTATIONAL SCIENCE & ENGINEERING

SAN DIEGO STATE UNIVERSITY

Structure enhancement diffusion and contour extraction for electron tomography of mitochondria

Carlos Bazán [a,*], Michelle Miller [b] and Peter Blomgren [b]

[a] *San Diego State University, Computational Science Research Center*

5500 Campanile Drive, San Diego, CA 92182-1245

Phone 619.594.2268, Fax 619.594.2459

[b] *San Diego State University, Department of Mathematics & Statistics*

5500 Campanile Drive, San Diego, CA 92182-7720

Phone 619.594.2602, Fax 619.594.6746

Abstract

The interpretation and measurement of the structural architecture of mitochondria depend heavily upon the availability of good software tools for filtering, segmenting, extracting, measuring and classifying the features of interest. Images of mitochondria contain many flow-like patterns and they are usually corrupted by large amounts of noise. Thus, it becomes necessary to enhance them by denoising and closing interrupted structures. We introduce a new approach based on anisotropic nonlinear diffusion and bilateral filtering for electron tomography of mitochondria. It allows noise removal and structure closure at certain scales, while preserving both the orientation and magnitude of discontinuities. This technique facilitates image enhancement for subsequent segmentation, contour extraction, and improved visualization of the complex and intricate mitochondrial morphology. We perform the extraction of the structure-defining contours by employing a variational level set formulation. The propagating front for this approach is an approximate signed distance function which does not require expensive re-initialization. The behavior of the combined approach is tested for visualizing the structure of a HeLa cell mitochondrion and the results we obtain are very promising.

Key words: Electron tomography, image processing, anisotropic nonlinear diffusion, bilateral filter

PACS: 68.37.-d, 07.05.Pj, 87.63.lm

* Corresponding author.

Email addresses: `carlos.bazan@sdsu.edu` (Carlos Bazán),
`miller.michelle.m@gmail.com` (Michelle Miller), `blomgren@terminus.sdsu.edu` (Peter Blomgren).

1 Introduction

To date, it is firmly established that mitochondrial function plays an important role in the regulation of apoptosis (Green and Reed, 1998; Obeid et al., 2007). For instance, following a variety of cell death signals, mitochondria exhibit early alterations in function and morphologic changes, such as the opening of the permeability transition pore or mitochondrial megachannel (Frank et al., 2001; Zamzami et al., 2007). There is also strong evidence that defects in function may be related to many of the most common diseases of aging, such as Alzheimer dementia, Parkinson's disease, type II diabetes mellitus, stroke, atherosclerotic heart disease, and cancer. This is founded on the observation that mitochondrial function undergoes measurable disturbance accompanied by drastic morphologic alterations in the presence of these multisystem diseases (Frey et al., 2006; Munnich and Rustin, 2001; Tandler et al., 2002).

Concurrent with the aforementioned conceptual advances there has been a significant increase in the types of tools available to study the correlation between mitochondrial structure and function. Along with the now classic methods for isolating mitochondria and assaying their biochemical properties, there are new and powerful methods for visualizing, monitoring, and perturbing mitochondrial function while assessing their genetic consequences (Marco et al., 2004; Pon and Schon, 2007). Electron tomography (ET) has allowed important progress in the understanding of mitochondrial structure. This imaging technique currently provides the highest three-dimensional (3D) resolution of the internal arrangement of mitochondria in thick sections (Henderson, 2004; Perkins and Frey, 1999). Nevertheless, the interpretation and measurement of the structural architecture of mitochondria depend heavily on the availability of good software tools for filtering, segmenting, extracting, measuring and classifying the features of interest (Frey et al., 2002; Perkins et al., 1997).

This paper is organized as follows: section 2 presents an overview of anisotropic non-linear diffusion models in image processing in general, and in electron microscopy in particular. The level set method is also presented briefly as it is applied to the extraction of contours in images. In section 3 we propose a new image smoothing and edge detection technique for electron tomography as an extension to the model proposed by Bazan and Blomgren (2007). This approach employs a combination of anisotropic nonlinear diffusion and bilateral filtering. In section 4 we exhibit the performance of the combined approach for visualizing the structure of a HeLa cell mitochondrion with very promising results. We end this paper with a summary and discussion in section 5.

2 Related Work

In this section we present an overview of anisotropic nonlinear diffusion models in image processing in general, and in electron microscopy in particular. The level set method is also presented briefly as it is applied to the extraction of contours in images. We only review here the works that serve as background to the model we propose in section 3. For an excellent and comprehensive survey of diffusion methods in image processing we refer the interested reader to the book by Weickert (Weickert, 1998) and the references therein. Two very good references for the level set method are the books by Osher and Fedkiw (2003) and by Sethian (1999).

2.1 Nonlinear Diffusion in Image Processing

Nonlinear diffusion is a very powerful image processing technique used for the reduction of noise and enhancement of structural features. It was first introduced to the

image processing community by Perona and Malik (1990) as an attempt to overcome the shortcomings of linear diffusion processes, namely the blurring of edges and other localization problems. Their model accomplishes this by applying a process that reduces the diffusivity in areas of the image with higher likelihood of belonging to edges. This likelihood is measured by a function of the local gradient $|\nabla u|$. The model can be written as

$$u_t - \nabla \cdot \left(g \left(|\nabla u|^2 \right) \cdot \nabla u \right) = 0, \tag{1}$$

for $t > 0$, on a closed domain Ω, with the observed image as initial condition $u(\mathbf{x}, 0) = u_0(\mathbf{x})$, and homogeneous Neumann boundary conditions $\langle g \cdot \nabla u, \mathbf{n} \rangle = 0$, on the boundary $\partial \Omega$. Here, $\mathbf{n}$ denotes the outward normal to the domain's boundary $\partial \Omega$, and $\langle \cdot, \cdot \rangle$ indicates the inner product $\int_{\partial \Omega} (g \cdot \nabla u) \cdot \mathbf{n}$. In this model the diffusivity has to be such that $g\left(|\nabla u|^2\right) \to 0$ when $|\nabla u| \to \infty$ and $g\left(|\nabla u|^2\right) \to 1$ when $|\nabla u| \to 0$.

Notwithstanding the practical success of the Perona-Malik model, it presents some serious theoretical problems such as (i) ill-posedness (Nitzberg and Shiota, 1992; Weickert and Schnörr, 2000); (ii) non-uniqueness and instability (Catté et al., 1992; Kichenassamy, 1997); (iii) excessive dependence on numerical regularization (Benhamouda, 1994; Fröhlich and Weickert, 1994). The last observation motivated an enormous amount of research towards the incorporation of the regularization directly into the PDE, to avoid too much implicit reliance on the numerical schemes. A variety of spatial, spatio-temporal, and temporal regularization procedures have been proposed over the years (Alvarez et al., 1992; Catté et al., 1992; Cottet and Germain, 1993; Weickert, 2001, 1994b, 1996b; Whitaker and Pizer, 1993). In subsection 2.2 we describe one of the variants to the Perona-Malik model that has been successfully used in electron microscopy, and in section 3 we propose a new model based on a

5

combination of anisotropic nonlinear diffusion and bilateral filtering.

2.2   Anisotropic Nonlinear Diffusion in Electron Tomography

One way of introducing regularization to the Perona-Malik model is through anisotropic diffusion. The main advantage of anisotropic diffusion models over their inhomogeneous isotropic counterparts is that they not only account for the modulus of the edge detector, but also its directional information. Isotropic diffusion will inhibit diffusion near edges, making it hard to eliminate noise near them. Anisotropic diffusion, on the other hand, will allow diffusion parallel to the edges while avoiding diffusing perpendicular to them.

Förstner and Gülch (1987) and Bigün and Granlund (1987) concurrently introduced the matrix field of the structure tensor for image processing and it is the basis for today's anisotropic diffusion models. The main idea behind these models is to construct the orthogonal system of eigenvectors $\mathbf{v}_1$, $\mathbf{v}_2$, of the diffusion tensor $\mathbf{D}_\sigma$ in such way that they will reveal the presence of edges, i.e., $\mathbf{v}_1 \parallel \nabla u_\sigma$ (parallel) and $\mathbf{v}_2 \perp \nabla u_\sigma$ (perpendicular). Then one chooses appropriate (corresponding) eigenvalues that will allow smoothing parallel to the edges and avoid doing so across them. The diffusion tensor $\mathbf{D}_\sigma$ steers the diffusion process in such a way that the eigenvectors prescribe the diffusion directions and the corresponding eigenvalues determine the amount of diffusion along these directions. Cottet and Germain (1993) and Weickert (1994a, 1996a) were among the first authors to propose anisotropic nonlinear diffusion models for image processing. Weickert (1994c) has also provided a mathematical foundation for continuous anisotropic nonlinear diffusion filtering as a scale-space transformation, adequate for simplifying images without renouncing the edge enhancing capability.

Anisotropic nonlinear diffusion in electron microscopy was introduced by Frangakis and Hegerl (2001, 1999). They proposed solving

$$u_t - \nabla \cdot (\mathbf{D}_\sigma \cdot \nabla u) = 0, \qquad \text{on } \Omega \times (0, \infty),$$

$$u(\mathbf{x}, 0) = u_0(\mathbf{x}), \qquad \text{on } \Omega, \qquad (2)$$

$$\langle g \cdot \nabla u, \mathbf{n} \rangle = 0, \qquad \text{on } \partial\Omega \times (0, \infty),$$

where the diffusivity matrix $\mathbf{D}_\sigma$ is structured as follows:

$$\mathbf{D}_\sigma = \begin{bmatrix} \mathbf{v}_1 & \mathbf{v}_2 & \mathbf{v}_3 \end{bmatrix} \begin{bmatrix} \lambda_1 & 0 & 0 \\ 0 & \lambda_2 & 0 \\ 0 & 0 & \lambda_3 \end{bmatrix} \begin{bmatrix} \mathbf{v}_1^{\mathrm{T}} \\ \mathbf{v}_2^{\mathrm{T}} \\ \mathbf{v}_3^{\mathrm{T}} \end{bmatrix}. \qquad (3)$$

The vectors $\mathbf{v}_i$ are the eigenvectors of the image's structure tensor $\mathbf{J}_\sigma = \nabla u_\sigma \cdot \nabla u_\sigma^{\mathrm{T}}$ or its convolved version $\mathbf{J}_\rho = G_\rho * \mathbf{J}_\sigma$, where $u_\sigma = G_\sigma * u$ and G_σ, G_ρ are Gaussian kernels of width σ, ρ, respectively. The parameters λ_i are functions of the eigenvalues, $\mu_1 \geq \mu_2 \geq \mu_3$, of the structure tensor $\mathbf{J}_\sigma$ (or $\mathbf{J}_\rho$). Together, the eigenvalues μ_i and the eigenvectors $\mathbf{v}_i$, characterize the local structural features of the image u, within a neighborhood of size $O(\rho)$. Each eigenvalue μ_i reflects the variance of the gray level in the direction of the corresponding eigenvector $\mathbf{v}_i$, while each parameter λ_i controls the diffusion flux in the direction of $\mathbf{v}_i$ and has to be chosen carefully.

Based on the works of Weickert (1998, 1999a,b), the authors in (Frangakis and Hegerl, 2001, 1999) chose the parameters λ_i to create a hybrid model that combines both edge enhancing diffusion (EED) and coherence enhancing diffusion (CED). EED is based on the directional information of the eigenvectors of the structure tensor $\mathbf{J}_\sigma$, and its aim is to preserve and enhance edges. CED is based on the directional information of the eigenvectors of the convolved structure tensor $\mathbf{J}_\rho$, and is intended for improving flow-like structures and curvilinear continuities. For EED, Frangakis and Hegerl (2001,

1999) chose the parameters λ_i following the Perona-Malik model:

$$\lambda_1 = \lambda_2 = g\left(|\nabla u_\sigma|^2\right),$$
$$\lambda_3 = 1, \tag{4}$$

while for CED, they are defined according to

$$\lambda_1 = \lambda_2 = \alpha,$$

$$\lambda_3 = \begin{cases} \alpha & \text{if } \mu_1 = \mu_3 \\ \alpha + (1-\alpha)\exp\left(-C\big/(\mu_1 - \mu_3)^2\right) & \text{else}, \end{cases} \tag{5}$$

with user-defined free parameters α (regularization constant, typically set to 10^{-3}) and $C > 0$. Structures with $(\mu_1 - \mu_3)^2 > C$ will be regarded as line-like patterns and will be enhanced.

To combine the advantages of EED and CED, the approach presented by Frangakis and Hegerl (2001, 1999) uses a switch based on comparing an ad hoc threshold parameter to the local relation between structure and noise $(\mu_1 - \mu_3)$. The threshold parameter is based on the mean value of $(\mu_1 - \mu_3)$ in a subvolume of the image containing only noise. EED is used when the difference $(\mu_1 - \mu_3)$ is smaller than the threshold parameter. When it is larger, the model switches to CED. In a separate publication, Frangakis et al. (2001) applied the hybrid model to two-dimensional (2D) and 3D electron tomography data and compared it with conventional methods as well as with wavelet transform filtering. They concluded that the model exhibits excellent performance at lower frequencies, achieving considerable improvement in the signal-to-noise-ratio (SNR) that greatly facilitated the posterior segmentation and visualization.

Fernández and Li (2003, 2005) proposed a variant to the model by Frangakis and Hegerl (2001, 1999) for ET filtering by anisotropic nonlinear diffusion, capable of re-

ducing noise while preserving both planar and curvilinear structures. They provided their model with a background filtering mechanism that highlights the interesting biological structural features and a new criterion for stopping the iterative process. The CED model presented in Eq. (5) diffuses unidirectionally along the direction of minimum change, $\mathbf{v}_3$, and efficiently enhances line-like structures (where $\mu_1 \approx \mu_2 \gg \mu_3$). It was argued by Fernández and Li (2003) that a significant number of structural features from biological specimens resemble plane-like structures at local scale. Therefore, they defined a set of metrics to discern whether the features are plane-like, line-like or isotropic. The metrics they defined are:

$$P_1 = \frac{\mu_1 - \mu_2}{\mu_1}, \qquad P_2 = \frac{\mu_2 - \mu_3}{\mu_1}, \qquad P_3 = \frac{\mu_3}{\mu_1}, \qquad (6)$$

which satisfy $0 \leq P_i \leq 1$, $\forall i$ and $P_1 + P_2 + P_3 = 1$. In Eq. (6) μ_1, μ_2 and μ_3 are the eigenvalues of the convolved structure tensor $\mathbf{J}_\rho$. These metrics are such that when $P_1 > P_2$ and $P_1 > P_3$, we have a plane-like structure; when $P_2 > P_1$ and $P_2 > P_3$, we have a line-like structure; and when $P_3 > P_1$ and $P_3 > P_2$, we have an isotropic structure. To achieve planar enhancing diffusion, Fernández and Li (2003, 2005) modified Eq. (5) as follows:

$$\lambda_1 = \alpha,$$

$$\lambda_2 = \begin{cases} \alpha & \text{if } \mu_1 = \mu_2 \\ \alpha + (1 - \alpha) \exp\left(-C_2 \big/ (\mu_1 - \mu_2)^2\right) & \text{else,} \end{cases}$$

$$\lambda_3 = \begin{cases} \alpha & \text{if } \mu_1 = \mu_3 \\ \alpha + (1 - \alpha) \exp\left(-C_3 \big/ (\mu_1 - \mu_3)^2\right) & \text{else.} \end{cases} \qquad (7)$$

For the case of isotropic structure, the model employs what Fernández and Li (2005) call 'background diffusion' based on Gaussian smoothing.

Brox and Weickert (2002) argued that the linear structure tensor $\mathbf{J}_\rho$ derived from $\mathbf{J}_\sigma$

by smoothing each component by a Gaussian kernel with standard deviation ρ, closes structures of a certain scale very well and removes the noise appropriately. However, it only preserves orientation discontinuities and does not preserve magnitude discontinuities, causing object boundaries to dislocate. Brox et al. (2005) argued that as soon as the orientation in the local neighborhood is not homogeneous, the local neighborhood induced by the Gaussian filter integrates ambiguous structure information. This information might not belong together and could lead to erroneous estimations. They proposed two alternatives to overcome this problem. The first solution involves the use of robust statistics for choosing one of the ambiguous orientations (van den Boomgaard and van de Weijer, 2002). The second solution is to adapt the neighborhood to the data by using the Kuwahara-Nagao operator (Bakker et al., 1999; Kuwahara et al., 1976; Nagao and Matsuyama, 1979). van den Boomgaard (2002) showed that the classic Kuwahara-Nagao operator can be regarded as a 'macroscopic' version of a PDE image evolution that combines linear diffusion with morphologic sharpening. Other similar approaches involve the choosing of the local neighborhood via adaptive Gaussian windows (Middendorf and Nagel, 2001, 2002; Nagel and Gehrke, 1998), and the use of nonlinear diffusion that can perform data-adaptive smoothing that prevents the integration of ambiguous data (Brox et al., 2004, 2006; Weickert and Brox, 2002).

Brox and Weickert (2002) proposed to address the aforementioned problem by replacing the Gaussian convolution by a discontinuity preserving diffusion method. This is obtained by considering the structure tensor $\mathbf{J}_\sigma$ as and initial matrix field that is evolved under the diffusion equation

$$\partial_t u_{ij} - \nabla \cdot \left(\mathbf{D} \left(\left(\nabla_\sigma \sqrt[4]{\sum_{k,l} u_{kl}^2} \right) \cdot \left(\nabla_\sigma \sqrt[4]{\sum_{k,l} u_{kl}^2} \right)^{\mathrm{T}} \right) \cdot \nabla u_{ij} \right) = 0, \qquad (8)$$

$\forall\, i, j$, where the evolving matrix field $u_{ij}(\mathbf{x}, t)$ uses $\mathbf{J}_\sigma(\mathbf{x})$ as initial condition for $t = 0$. The matrix $\mathbf{D}(A) = \mathbf{T}(g(\lambda_i)) \cdot \mathbf{T}^{\mathrm{T}}$ is the diffusion tensor for $A = \mathbf{T}(\lambda_i) \cdot \mathbf{T}^{\mathrm{T}}$.

The latter represents a principal axis transformation of A with the eigenvalues λ_i as the elements of a diagonal matrix, $\text{diag}\,(\lambda_i)$, and the normalized eigenvectors as the columns of the orthogonal matrix, $\mathbf{T}$. For the diffusivity, $g = 1 - \exp\left(-c\big/(s/\lambda)^8\right)$, for $c > 0$ and λ the contrast parameter. In Eq. (8), ∇_σ denotes the nabla operator where Gaussian derivatives with standard deviation σ are employed. This approach tends to prevent boundary dislocations while keeping the desirable properties of the linear structure tensor. In section 3 we introduce a new approach based on anisotropic nonlinear diffusion and bilateral filtering for electron tomography. It allows noise removal and structure closure at certain scales, while preserving both the orientation and magnitude of discontinuities

2.3   Contour Extraction Using the Level Set Method

Osher and Sethian (1988) developed a framework relying on a PDE approach for modeling propagating interfaces. These methods have been applied to recover shapes of 2D and 3D objects from visual data, as shown by Malladi et al. (1996). This modeling scheme makes no a priori assumptions about the object's shape and starts with an arbitrary function, propagating it in the direction normal to the curve along its gradient field with a certain speed, to recover shapes in the image.

The level set formulation allows both forward and backward motion of the initial front through the creation of a higher dimensional function $\phi(\mathbf{x}, t)$ where the initial position of the front is embedded as the zero level set. The evolution of the function $\phi(\mathbf{x}, t)$ is then linked to the propagation of the front itself through a time-dependent initial value problem. Thus, given any time t, the position of the front is given by the zero level set of the time-dependent level set function $\phi\left(\Gamma\left(t\right) = \{\mathbf{x}\,|\,\phi\left(\mathbf{x}, t\right) = 0\}\right)$. The evolution equation, or level set equation (Sethian, 1999), for ϕ given by Osher

11

and Sethian (1988) can be written as follows:

$$\phi_t + F\,|\nabla\phi| = 0, \qquad \text{given } \phi\left(\mathbf{x}, t = 0\right). \tag{9}$$

Many implementations (Osher and Fedkiw, 2003) of the level set method utilize a zero (or initial) level set such that $\phi(\mathbf{x}, t = 0) = \pm d(\mathbf{x})$, where $\pm d(\mathbf{x})$ is the signed distance to $\Gamma\left(0\right)$. This choice of ϕ allows for both conceptual simplifications and computational savings (Osher and Fedkiw, 2003, section 4.2). Throughout the evolution of the front, in order to avoid the formation of shocks, very flat shapes, and/or very sharp shapes, a re-initialization process is often used periodically to restore a signed distance function. One approach widely used for re-initialization is to solve the equation

$$\phi_t = sign\left(\phi_0\right)\left(1 - |\nabla\phi|\right), \tag{10}$$

given the function to be re-intialized ϕ_0 and the sign function $sign(\phi)$ (Osher and Fedkiw, 2003). The process of re-initialization, using the PDE-based method above or similar variation, can be complicated and expensive. There is no simple way to determine how and when the level set function should be re-initialized to a signed distance function.

Li et al. (2005) presented a variational formulation whose propagating front is an approximate signed distance function yet does not require re-initialization. The variational energy functional consists of both an internal energy term that forces the level set function to be kept as an approximate signed distance function, and an external energy term that drives the zero level set toward the sought object contours in the image. The total energy functional is given by

$$\mathcal{E}\left(\phi\right) = \mu\mathcal{P}\left(\phi\right) + \mathcal{E}_{g,\lambda,\nu}\left(\phi\right). \tag{11}$$

The first term in the sum is the internal energy. It helps prohibit the deviation of ϕ from a signed distance function, where $\mu > 0$ is the parameter controlling the effect

of the penalizing the deviation. $\mathcal{P}(\phi)$ is a metric that characterizes how close ϕ is to a signed distance function whose definition follows from Eq. (10):

$$\mathcal{P}(\phi) = \frac{1}{2} \int_\Omega \left(|\nabla \phi| - 1 \right)^2 d\mathbf{x}. \tag{12}$$

The second term in the sum of Eq. (11) is the external energy term that moves the zero level curve toward the object boundaries. Given an image u we can define the following edge indicator function where G_σ is the Gaussian kernel with standard deviation σ:

$$g = \frac{1}{1 + |\nabla G_\sigma * u|^2}. \tag{13}$$

With this we can further specify our external energy term:

$$\mathcal{E}_{g,\lambda,\nu}(\phi) = \lambda \mathcal{L}_g(\phi) + \nu \mathcal{A}_g(\phi) \tag{14}$$

for constants: $\lambda > 0$, ν and terms: $\mathcal{L}_g(\phi) = \int_\Omega g\delta(\phi) |\nabla \phi| d\mathbf{x}$ and $\mathcal{A}_g(\phi) = \int_\Omega gH(-\phi) d\mathbf{x}$ where $\delta(\cdot)$ is the univariate Dirac function and $H(\cdot)$ is the Heaviside function. The energy term $\mathcal{L}_g(\phi)$ computes the length of the zero level curve of ϕ while $\mathcal{A}_g(\phi)$ is the weighted area on the interior of the zero level set and speeds up the curve evolution. The coefficient ν serves to control both the speed and direction of the curve propagation and should be chosen appropriately depending on the relative location of the initial contour to the object of interest. For an initial contour outside the object, ν should be a negative value so that the contours may shrink to the object boundary; whereas, a positive value should be chosen for ν if the initial contour is inside the object so that the contours might expand to the boundary.

The use of this energy functional completely eliminates the need for the expensive re-initialization as the evolution of the level set function is the gradient flow that minimizes the overall energy functional. The internal energy term maintains the level set function as an approximate signed distance function while the external energy

term drives the propagation. The evolution equation is determined using calculus of variations to differentiate $\mathcal{E}$ and setting its Gâteaux derivative equal to zero, yielding the steepest descent process for minimization of the functional $\mathcal{E}$:

$$\frac{\partial \phi}{\partial t} = \mu \left(\nabla^2 \phi - \nabla \cdot \left(\frac{\nabla \phi}{|\nabla \phi|} \right) \right) + \lambda \delta \left(\phi \right) \nabla \cdot \left(g \frac{\nabla \phi}{|\nabla \phi|} \right) + \nu g \delta \left(\phi \right). \qquad (15)$$

3 Anisotropic Nonlinear Diffusion and Bilateral Filter in Electron Tomography

In subsection 2.2 we discussed the application of anisotropic nonlinear diffusion in electron tomography. The approach used by Frangakis and Hegerl (2001, 1999) and Fernández and Li (2003, 2005) is based on a hybrid EED/CED denoising mechanism that performs very well on data containing low– to mid-frequency signal components. The technique greatly facilitates image enhancement for subsequent segmentation and improved visualization of complex biological specimens. In this section we propose a new image smoothing and edge detection technique for electron tomography as an extension to the model proposed by Bazan and Blomgren (2007). This approach employs a combination of anisotropic nonlinear diffusion and bilateral filtering. Jiang et al. (2003) introduced bilateral filtering for the removal of noise from biological electron microscopy data. They showed that bilateral filtering is a very effective mechanism for suppressing the noise in tomograms while preserving high resolution secondary structure features. Our model aims at incorporating the best of both approaches in a single computationally robust implementation. The model is equipped with the diffusion stopping criterion proposed by Bazan and Blomgren (2007), based on the second derivative of the correlation between the noisy image and the filtered image (see Appendix A for details on this diffusion stopping criterion).

14

3.1 Local Structure Analysis

The structure tensor of a 3D tomogram u is a symmetric positive semidefinite matrix, $\mathbf{J}_\sigma$. This structure tensor is the most stable and reliable descriptor of local structure of an image (Weickert, 1995). Similar to the approach in (Bazan and Blomgren, 2007), we propose using a refined estimate of the gradient of u at voxel $\mathbf{x} = (x, y, z)$ obtained by applying a bilateral filter in place of the Gaussian kernel. Bilateral filtering is a technique for smoothing images while preserving edges. The first application of this method is attributed to Aurich and Weule (1995) and it was subsequently rediscovered by Smith and Brady (1997) and Tomasi and Manduchi (1998). Since its introduction, the bilateral filter has been successfully employed in various contexts (Aleksic et al., 2006; Bae et al., 2006; Bennet and McMillan, 2005; Eisemann and Durand, 2004; Petschnigg et al., 2004; Ramanath and Snyder, 2003; Winnermöller et al., 2006). The bilateral filter's characteristics and behavior have been the subjects of extensive theoretical studies that have made bilateral filtering a fairly well understood process (Barash and Comaniciu, 2004; Buades et al., 2006; Mrázek et al., 2006; Paris and Durand, 2006).

The basic idea underlying bilateral filtering is to combine domain and range filtering, thereby enforcing both geometric and photometric locality. The model can be expressed as

$$G_{bf} * u\left(\mathbf{x}\right) = \frac{1}{W\left(\mathbf{x}\right)} \int_\Omega G_{\sigma_d}\left(\xi, \mathbf{x}\right) G_{\sigma_r}\left(u\left(\xi\right), u\left(\mathbf{x}\right)\right) u\left(\xi\right) d\xi, \tag{16}$$

with the normalization constant

$$W\left(\mathbf{x}\right) = \int_\Omega G_{\sigma_d}\left(\xi, \mathbf{x}\right) G_{\sigma_r}\left(u\left(\xi\right), u\left(\mathbf{x}\right)\right) d\xi. \tag{17}$$

Typically, G_{σ_d} will be a spatial Gaussian that decreases the influence of distant pixels,

while G_{σ_r} will be a range Gaussian that decreases the influence of pixels $u\left(\xi\right)$ with intensity values that are very different from those of $u\left(\mathbf{x}\right)$, e.g.

$$G_{\sigma_d} = \exp\left(-\frac{|\xi - \mathbf{x}|^2}{2\sigma_d^2}\right), \qquad G_{\sigma_r} = \exp\left(-\frac{|u\left(\xi\right) - u\left(\mathbf{x}\right)|^2}{2\sigma_r^2}\right). \qquad (18)$$

The parameters σ_d and σ_r dictate the amount of filtering applied in the domain and the range of the image, respectively.

The new structure tensor is therefore $\mathbf{J}_{bf} = \nabla u_{bf} \cdot \nabla u_{bf}^{\mathrm{T}}$. The image's local structural features can be determined by performing the eigen-analysis of the structure tensor $\mathbf{J}_{bf}$ where, as before, the eigenvalues provide the average contrast along the eigen-directions, and the corresponding eigenvectors give the preferred local orientations. We will take advantage of the information provided by the structure tensor at each voxel $\mathbf{x}$, to devise a robust anisotropic structure enhancement model for 3D electron tomograms of mitochondria. Images of mitochondria contain many flow-like patterns and they are often perturbed large amounts of noise (including the artifacts related to the limited tilt range.) Thus, it becomes necessary to denoise and enhance them by closing interrupted structures. To exploit the coherence and curvilinear continuity while connecting possible interrupted lines and planes, we will average the structure tensor $\mathbf{J}_{bf}$ over a region by applying bilateral filtering in the form $\overline{\mathbf{J}}_{bf} = G_{bf} * \mathbf{J}_{bf}$. The directional information is thereby averaged, although the structure of the region is still preserved.

3.2 Diffusion Tensor Construction

The diffusion tensor, $\mathbf{D}_{bf} \in \mathbb{R}^{3\times3}$, controls the smoothing across the 3D tomogram. Similar to how it was done above, we define the diffusion tensor as a function of the

structure tensor $\overline{\mathbf{J}}_{bf}$,

$$\mathbf{D}_{bf} = \begin{bmatrix} \mathbf{v}_1 & \mathbf{v}_2 & \mathbf{v}_3 \end{bmatrix} \begin{bmatrix} \lambda_1 & 0 & 0 \\ 0 & \lambda_2 & 0 \\ 0 & 0 & \lambda_3 \end{bmatrix} \begin{bmatrix} \mathbf{v}_1^{\mathrm{T}} \\ \mathbf{v}_2^{\mathrm{T}} \\ \mathbf{v}_3^{\mathrm{T}} \end{bmatrix}, \tag{19}$$

where $\mathbf{v}_i$ are the structure tensor's eigenvectors. The eigenvalues of the diffusion tensor, λ_i, define the strength of the smoothing along the eigen-directions, $\mathbf{v}_i$, and allow the application of different diffusion processes: (i) Linear diffusion or Gaussian smoothing is applied when $\lambda_i = 1, \forall i$; (ii) Nonlinear diffusion is applied if $\lambda_i = g\left(|\nabla u|^2\right), \forall i$; (iii) Anisotropic diffusion can be applied by setting the values λ_i so they would reflect the image's underlying local structure.

As presented earlier, it is now common to use a hybrid approach that switches the diffusion process from EED to CED and vice versa, based on selected ad hoc thresholds. Switching to a third diffusion mode, Gaussian diffusion (GD), in areas where the image becomes predominantly isotropic (based on another ad hoc threshold) has also been suggested. We propose to use the anisotropic diffusion process where the model switches among the three modes, EED/CED/GD, automatically based on information extracted locally from the signal. The model can be regarded as 'structure enhancing diffusion' (SED), where the eigenvalues are defined as

$$\lambda_1 = g\left(|\nabla u_{bf}|^2\right),$$

$$\lambda_2 = \begin{cases} g\left(|\nabla u_{bf}|^2\right) & \text{if } \mu_1 = \mu_2 \\ g\left(|\nabla u_{bf}|^2\right) + \left(1 - g\left(|\nabla u_{bf}|^2\right)\right) \exp\left(-C_2 \big/ (\mu_1 - \mu_2)^2\right) & \text{else,} \end{cases} \tag{20}$$

$$\lambda_3 = \begin{cases} g\left(|\nabla u_{bf}|^2\right) & \text{if } \mu_1 = \mu_3 \\ g\left(|\nabla u_{bf}|^2\right) + \left(1 - g\left(|\nabla u_{bf}|^2\right)\right) \exp\left(-C_3 \big/ (\mu_1 - \mu_3)^2\right) & \text{else.} \end{cases}$$

Coherence measures $(\mu_1 - \mu_2)^2$ and $(\mu_1 - \mu_3)^2$ are computed based on the eigenvalues of the averaged structure tensor $\overline{\mathbf{J}}_{bf}$, and the parameters C_2 and C_3 act as thresholds such that structures where $(\mu_1 - \mu_2)^2 > C_2$ and $(\mu_1 - \mu_3)^2 > C_3$ are regarded as planar patterns, while structures where $(\mu_1 - \mu_2)^2 < C_2$ and $(\mu_1 - \mu_3)^2 > C_3$ are regarded as linear patterns. In practice, the logical 'if $\mu_1 = \mu_2$ then' and 'if $\mu_1 = \mu_3$ then' are unnecessary if we use $\exp\left(-C_2 \big/ \left((\mu_1 - \mu_2)^2 + \varepsilon\right)\right)$ and $\exp\left(-C_3 \big/ \left((\mu_1 - \mu_3)^2 + \varepsilon\right)\right)$, for small ε.

In Eq. (20), $g\left(|\nabla u_{bf}|^2\right)$ is a monotonically decreasing function such as Perona-Malik's

$$g\left(|\nabla u_{bf})|^2\right) = \frac{1}{1 + |\nabla u_{bf}|^2 \big/ \lambda^2}, \tag{21}$$

with $\lambda > 0$ the typical contrast threshold parameter. There are several ways to set this parameter. Perona and Malik (1990) suggested using the idea presented by Canny (1986) and set λ as a percentile, p, of the image gradient magnitudes at each iteration (they recommended the value $p = 90\%$.) A by-product of this approach is a decreasing λ, which has an stabilizing effect on the diffusion process (Mrázek, 2001).
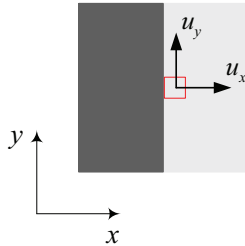
Fig. 1. Fragment of an image where an edge pixel's gradient has components $u_y = 0$ and $0 < |u_x| \leqslant 1$, depending on the gray values in the two regions.

The advantages of the proposed definitions for the diffusion tensor's eigenvalues become evident when we perform a 2D analysis of the behavior of λ_1 and λ_2. Assume we are standing on an edge pixel of an image $u \in [0, 1]$, as shown in Fig. 1. In this case, $u_y = 0$ and $0 < |u_x| \leqslant 1$, depending on the gray values in the two regions. The typical hybrid approach will use a chosen threshold to switch between EED and

CED (see Eq. (4) and Eq. (7)), and set the diffusion tensor's eigenvalues to: either $\lambda_1 = g\left(|\nabla u|^2\right)$ or $\lambda_1 = \alpha$; and either $\lambda_2 = 1$ or $\lambda_2 = \alpha + (1-\alpha)\exp\left(-C\big/(\mu_1 - \mu_2)^2\right)$. Assuming for example the values, $\alpha = 10^{-3}$ and $C = 4.5 \times 10^{-4}$, and considering that $(\mu_1 - \mu_2)^2 = \left(u_x^2 - u_y^2\right)^2 + 4\left(u_x u_y\right)^2$, we can plot λ_1 and λ_2 along $u_y = 0$ and interpret the following (see Fig. 2):
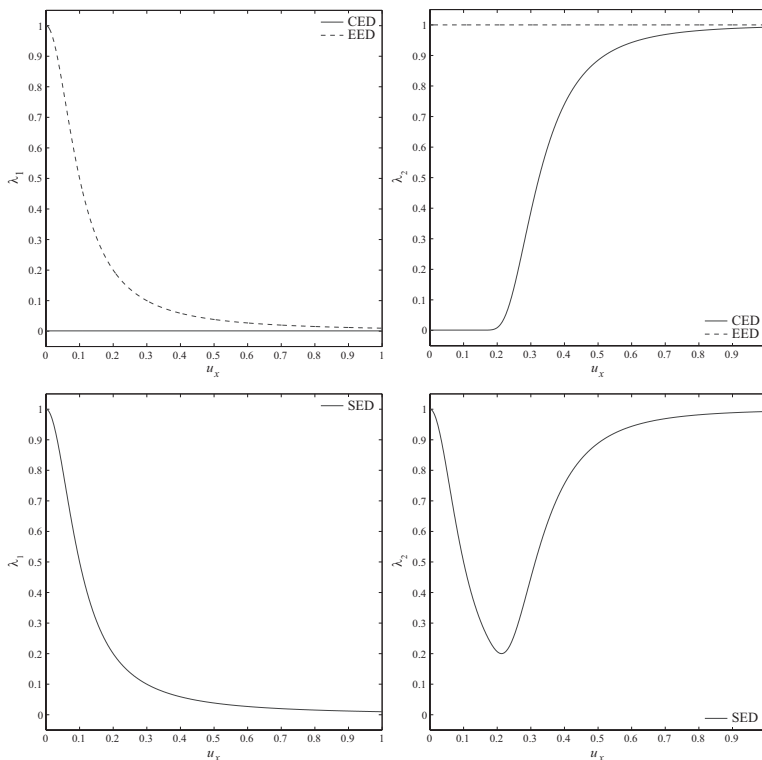
Fig. 2. Eigenvalues λ_1 and λ_2 for the EED, CED and SED models. The hybrid EED/CED model switches sharply between the EED and CED curves based on an ad hoc threshold.

(i) For high gradients, $|u_x| \to 1$, the EED, CED and SED models will assume similar values for λ_1, and so will the hybrid EED/CED and SED models;

(ii) For mid-range gradients, $0 < |u_x| < 1$, the values for λ_1 must increase to prevent diffusing across the edge. Since the EED/CED switch is a function of the gradient u_x, the hybrid EED/CED will switch from $\lambda_1 = \alpha$ to $\lambda_1 = g\left(|\nabla u|^2\right)$ in a sudden jump. After the switch, as $|u_x| \to 0$, both the hybrid EED/CED and SED models will set

19

the same values for λ_1;

(iii) For high gradients, $|u_x| \to 1$, the EED, CED and SED models will assume similar values for λ_2, and so will the hybrid EED/CED and SED models;

(iv) For mid-range gradients, $0 < |u_x| < 1$, the values for λ_2 must decrease to prevent creating artificially sharpened edges. Both the hybrid EED/CED and SED models will set the same values for λ_2 until the switch triggers and changes the hybrid EED/CED model to EED mode, and makes λ_2 sharply jump to a value of 1;

(v) As $|u_x| \to 0$, both models must set $\lambda_2 \to 1$ to assume GD mode. The hybrid EED/CED will switch from CED to EED where $\lambda_2 = 1$, while the SED model will asymptotically assume $\lambda_2 = 1$.

(vi) The above rationale for the 2D case extends naturally to 3D. Also, if a voxel belongs to a linear structure, $\mu_1 \approx \mu_2 \gg \mu_3$, then $(\mu_1 - \mu_2) \to 0$ and consequently the term $\exp\left(-C_2 \big/ (\mu_1 - \mu_2)^2\right) \to 0$, making the switch between planar and linear structures automatic.

4 Image Acquisition and Processing

4.1 Image Acquisition

The electron tomogram employed in our experiments corresponds to a HeLa cell and it was obtained from a 250 nm semi-thick section across a mitochondrion expressing cytochrome c-GFP. In the interest of research not discussed here, apoptosis was induced in the mitochondria with 100μM etoposide for 15 hours. The imaging occurred before the release of cytochrome c or loss of membrane potential allowing the mainte-

nance of normal mitochondrion profiles; however, the treatment caused elongation of the crista junctions. The use of a semi-thick section is advantageous because it allows accurate depiction of the inner membrane topology of the mitochondrion.

The microscope used was the FEI Tecnai 12 Transmission Electron Microscope (TEM) with magnification set at 11000. The EM tomography single-tilt series 3D reconstruction was obtained from the semi-thick sample by progressively tilting the specimen and recording images using a Teitz 214 digital camera. The tilting was conducted in increments of 2 degrees over an angular range of $\pm 60°$; the angular range is limited by the geometry of the apparatus that holds the sample. Once the tilt-series was collected on the digital camera, the IMOD Software Suite (Kremer et al., 1996) was used to process the images and obtain the 3D reconstruction of the electron tomogram.

3D models are constructed using the electron tomogram. The 3D tomogram can be represented as a series of parallel sections, one pixel thick, of constant z. (Here, the image pixel size is 1.27 nm.) Constructing the models then requires the tracing of the membrane profiles of the outer membrane, inner membrane, and cristae structures in each of many parallel sections of the tomogram. These tracings form a stack of membrane contours that, when input to a computer display program, create a 3D model that can be rotated and viewed at any angle Frey et al. (2002). The tracing of the mitochondrial structures in the tomogram is currently done manually. However, by applying the proposed variational level set algorithm, the process is made less tracer-dependent.

After the 3D tomogram of the HeLa cell mitochondrion has been reconstructed, we apply the algorithm described in section 3 for the removal of noise and the enhancement of the structural features. This step is critical for the posterior segmentation and extraction of the structure-defining contours. The problem to solve is

$$
\begin{aligned}
u_t - \nabla \cdot (\mathbf{D}_{bf} \cdot \nabla u) &= 0, & \text{on } \Omega \times (0, \infty), \\
u(\mathbf{x}, 0) &= u_0(\mathbf{x}), & \text{on } \Omega, \\
\langle \mathbf{D}_{bf} \cdot \nabla u, \mathbf{n} \rangle &= 0 & \text{on } \partial\Omega \times (0, \infty).
\end{aligned}
\tag{22}
$$

We adopt the following notation for the components of the diffusion tensor:

$$
\mathbf{D}_{bf} = \lambda_1 \mathbf{v}_1 \cdot \mathbf{v}_1^{\mathrm{T}} + \lambda_2 \mathbf{v}_2 \cdot \mathbf{v}_2^{\mathrm{T}} + \lambda_3 \mathbf{v}_3 \cdot \mathbf{v}_3^{\mathrm{T}} =
\begin{bmatrix}
d_{11} & d_{12} & d_{13} \\
d_{21} & d_{22} & d_{23} \\
d_{31} & d_{32} & d_{33}
\end{bmatrix},
\tag{23}
$$

then, we can expand Eq. (22) and write

$$
\begin{aligned}
u_t &- \partial_x (d_{11} u_x + d_{12} u_y + d_{13} u_z) \\
&- \partial_y (d_{21} u_x + d_{22} u_y + d_{23} u_z) \\
&- \partial_z (d_{31} u_x + d_{32} u_y + d_{33} u_z) = 0,
\end{aligned}
\tag{24}
$$

for $t > 0$, with the observed image as initial condition, and homogeneous Neumann boundary conditions. We can apply the standard explicit finite difference scheme using central difference to approximate the spatial derivatives, and forward difference to approximate the time derivative. The condition for stability, assuming $\delta \mathbf{x} = 1$, is

given by $\delta t = 1/6$ (Weickert et al., 1998). The update will be

$$
\begin{aligned}
u_{t+1} = u_t + \delta t \, [\, \partial_x \left(d_{11}u_x + d_{12}u_y + d_{13}u_z \right) \\
+ \left(d_{21}u_x + d_{22}u_y + d_{23}u_z \right) \\
+ \partial_z \left(d_{31}u_x + d_{32}u_y + d_{33}u_z \right) \,] .
\end{aligned}
\tag{25}
$$

Fig. 3 shows some results of the proposed approach applied to a slice taken from the 3D electron tomogram of the HeLa cell mitochondrion. The proposed approach achieves excellent noise reduction while preserving the salient edge features. In order to facilitate extraction of the structures, we synthetically enhance the contrast by applying the confidence connected segmentation algorithm (Meier et al., 1997). In this context, this simple region-growing segmentation method produces sufficiently good results for the extraction stage, but more flexible methods such as the watershed technique (Volkmann, 2002) or the Chan and Vese (2001) algorithm can easily be substituted. After segmentation, the features are extracted using the level set approach described in subsection 2.3.

4.3   Contour Extraction

We adopt the formulation by Li et al. (2005) presented in subsection 2.3 to extract the contours in the mitochondrion images. One significant advantage of this formulation is the liberty allowed in selecting the initial level set function. Traditionally, using level set methods requires the initial level set to be a signed distance function ϕ_0 so that re-initialization can be applied. However, with this need eliminated, a much
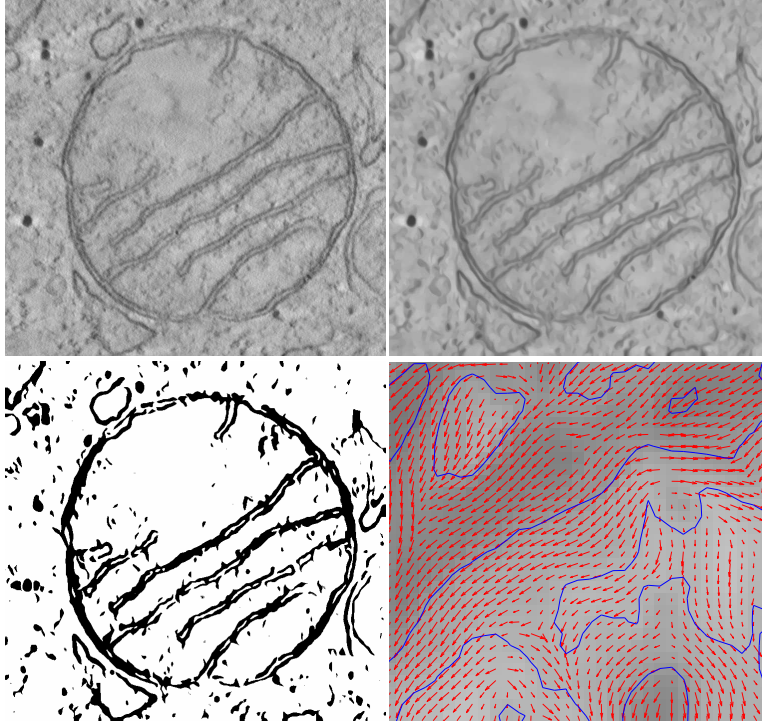
Fig. 3. Results of the proposed approach as a slice taken from the 3D electron tomogram of the HeLa cell mitochondrion. (upper-left) The noisy image. (upper-right) The filtered image after applying the structure enhancing diffusion method. We observe the good denoising capability of the proposed approach along with its excellent ability of preserving the edges. The filtered image facilitates the segmentation and posterior extraction of the structure's contours. (lower-left) The image segmented with the 'confident connected' segmentation algorithm. (lower-right) A fragment of the image's contours over which the structure tensor's term $\lambda_2 \mathbf{v}_2 \cdot \mathbf{v}_2^{\mathrm{T}}$ was superimposed.

simpler initial function may be defined:

$$
\phi_0(\mathbf{x}) = \begin{cases} -\eta, & \mathbf{x} \in \Omega_0 - \partial\Omega_0 \\ 0 & \mathbf{x} \in \partial\Omega_0 \\ \eta, & \Omega - \Omega_0 \end{cases}
\tag{26}
$$

given arbitrary Ω_0, a subset in the image domain Ω where $\partial\Omega_0$ is the set of points on the boundary of Ω_0, and $\eta > 0$. For our implementation $\eta = 4$ is selected; however, most any constant would work. For the purposes here we use a Dirac function $\delta(\mathbf{x})$ in Eq. (15) that is slightly smoothed. We define the regularized Dirac function $\delta_\epsilon(\mathbf{x})$ as follows

$$
\delta_\epsilon(\mathbf{x}) = \begin{cases} 0, & |\mathbf{x}| > \epsilon \\[2mm] \frac{1}{2\epsilon}\left(1 + \cos(\frac{\pi\mathbf{x}}{\epsilon})\right), & |\mathbf{x}| \leq \epsilon \end{cases} \tag{27}
$$

and utilize $\epsilon = 1.5$ for our implementation.
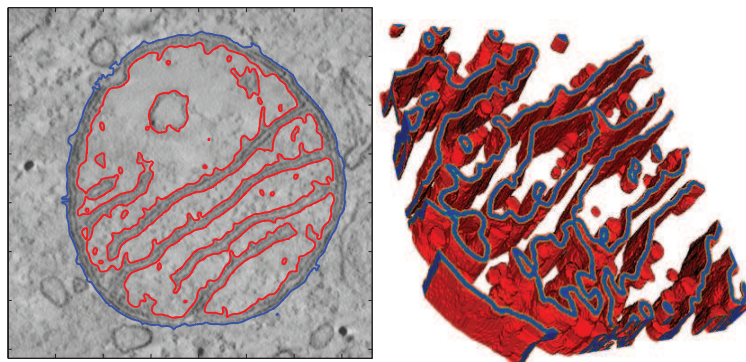
Fig. 4. (right) Results of extraction of the interior structures and outer membrane of a mitochondrion in an ET image. Algorithm was applied twice to the segmented image (Fig. 3) using parameters: $\lambda = 5.0$, $\mu = .04$, $\tau = 5.0$, $\nu = -25$ for interior initial contour and $\nu = 10$ for outer initial contour. Final contours were plotted on the original ET image slice. (left) Fragment of the 3D rendering of the structural contours extracted from the mitochondrion image.

In implementing the proposed level set method we carefully selected both our timestep τ and coefficient μ to be safely within the range required for stability ($\tau\mu < \frac{1}{4}$ as explained in Li et al. (2005)), $\tau = 5$ and $\mu = .04$. The level set functions were initialized as the function ϕ_0 defined by Eq. (10) with $\eta = 4$ using selected regions Ω_0. Fig. 4 shows the successful extraction of both the crista structures and outer

membrane of the 718×763 pixel mitochondrion image. Identification of the interior structures was conducted separately from the identification of the outer membrane due to the required opposite direction of contour evolution for each. In order that the initial contour expand to identify the inner structures ν was chosen to be -25 and the evolution required 53 iterations, whereas for the second initial contour, used to shrink to identify the outer membrane, η was chosen to be 10 and the evolution required 38 iterations. These selections allowed accurate visualization of the boundaries of interest. Note that the algorithm was run on the image in Fig. 3 (lower-left) and the resulting contours have been displayed on the original electron tomogram image slice.

5   Summary and Discussion

We have presented a multi-stage approach for extracting the mitochondrial structures from electron tomograms. In particular, we apply the strategy to a 3D tomogram of a HeLa cell mitochondrion.

In the initial reconstruction, or noise reduction phase, we propose a structure enhancing anisotropic nonlinear diffusion strategy: the local structure tensor $\mathbf{J}_{bf}$ is formed from the gradient information of a bilaterally smoothed version of the current image. In order to close gaps in structures caused by imaging limitations, the local structure tensor is further smoothed with a bilateral filter, forming a smoothed version of the structure tensor, $\overline{\mathbf{J}}_{bf}$. The eigenvectors $\mathbf{v}_i$, of the smoothed structure tensor form the basis for the diffusion tensor $\mathbf{D}_{bf}$, where the eigenvalues are prescribed so that there is a smooth interpolation, rather than a hard threshold switching of the diffusion characteristics between image areas of differing structure properties.

After the noise reduction phase, we synthetically enhance the contrast by applying

the confident-connected segmentation algorithm. Following which, structures are extracted using a level set formulation which includes a term that drives the level set function toward a signed distance function. This both simplifies the initialization of the algorithm and removes the need for re-initialization. Strictly speaking the segmentation stage is not necessary, as showcased in Li et al. (2005). However, for the image size (718×768) of the tomogram at hand, we found that the pre-segmentation relieved us from tedious parameter tuning in a two-dimensional parameter space, and thus reduced total runtime.

The extracted contours are visualized in Fig. 4. The left panel shows the successful result of extracting both the outer membrane and the inner structures; in the right panel we show a 3D-rendering of a 'stack' consisting of 25 extracted contours. The results are very encouraging. This computational approach is potentially much faster, and is more robust than hand-tracing of structures.

A   Appendix: Diffusion Stopping Criterion

Bazan and Blomgren (2007) proposed a new (very simple) diffusion-stopping criterion inspired by observation of the behavior of the correlation between the noise-free image and the filtered image, $\mathrm{corr}\,(f, u)$, and the correlation between the noisy image and the filtered image, $\mathrm{corr}\,(u_0, u)$. Although the former measure is only available in experimental settings it helps validate the usefulness of the latter. The nonlinear diffusion process starts from the observed (noisy) image, $u_0\,(\mathbf{x})$, and creates a set of filtered images, $u\,(\mathbf{x}, t)$, by gradually removing noise and details from scale to scale until, as $t \to \infty$, the image converges to a constant value. During this process the correlation between the noise-free image and the filtered image increases as the filtered image moves closer to the noise-free image. This behavior continues until it
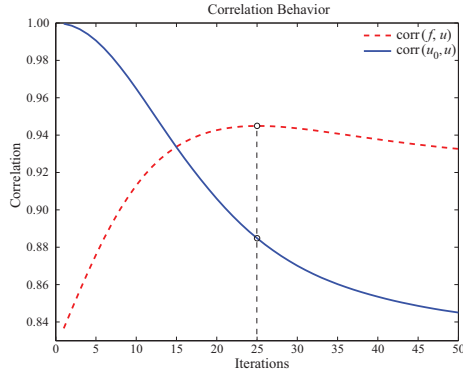
Fig. A.1. The correlation coefficient between the noise-free image and the filtered image increases as the filtered image moves closer to the noise-free image. When the measure reaches a peak it decreases as the filtered image moves slowly towards a constant value. The correlation coefficient between the noisy image and the filtered image decreases gradually from a value of 1.0 (perfect correlation), to a constant value as the filtered image becomes smoother.

reaches a peak from where the measure decreases as the filtered image moves slowly towards a constant value. During the same process the correlation between the noisy image and the filtered image decreases gradually from a value of 1.0 (perfect correlation), to a constant value, $\approx \operatorname{corr}(f, u_0)$, as the filtered image becomes smoother (see Fig. A.1). By comparing both measures we observe that as $\operatorname{corr}(f, u)$ reaches its maximum (best possible reconstructed image), the curvature of $\operatorname{corr}(u_0, u)$ changes sign. This suggests that a good stopping point of the diffusion process is where the second derivative of $\operatorname{corr}(u_0, u)$ reaches a maximum. The performance of the stopping criterion can be observed in Fig. A.1 along with the reconstructed images of 'Lena' and the 'Clown' (Fig. A.2). We observe that the stopping criterion is almost optimal, allowing the diffusion process to stop near the point where the three filtering methods reach their best possible image reconstructions.
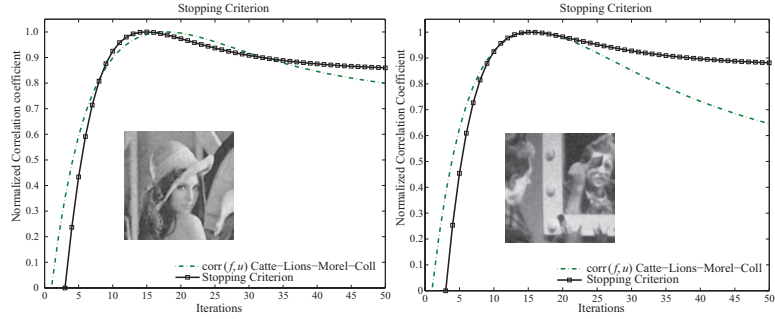
Fig. A.2. (left) Stopping criterion performance along with the reconstructed image of Lena using the Catté et al. (1992) model. The measure $\text{corr}(f, u)$ suggests stopping the diffusion process after 18 iterations, while the proposed stopping criterion suggests to stop the diffusion process after 15 iterations. (right) Stopping criterion performance along with the reconstructed image of the Clown using the Catté et al. (1992) model. The measure $\text{corr}(f, u)$ suggests stopping the diffusion process after 16 iterations, while the proposed stopping criterion suggests to stop the diffusion process after 15 iterations.

Acknowledgements

References

M. Aleksic, M. Smirnov, and S. Goma. Novel bilateral filter approach: Image noise reduction with sharpening. In *Proceeding of the Digital Photography II Conference*, pages 141-147. SPIE, 2006.

L. Alvarez, P.L. Lions, and J.M. Morel. Image selective smoothing and edge detection by nonlinear diffusion, II. *SIAM Journal on Numerical Analysis*, 29(3):845-866, 1992.

V. Aurich and J. Weule. Non-linear Gaussian filters performing edge preserving diffusion. In *Proceedings of DAGM Symposium*, volume 17, pages 538-545. Deutsche Arbeitsgemeinschaft für Mustererkennung, 1995.

S. Bae, S. Paris, and F. Durand. Two-scale tone management for photographic look. *ACM Transactions on Graphics*, 25(3):637-645, 2006.

P. Bakker, L. van Vliet, and P. Verbeek. Edge preserving orientation adaptive filtering. In M. Boasson, J. Kaandorp, J. Tonino, and M. Vosselman, editors, *Proceedings of 5th Annual Conference of the Advanced School for Computing and Imaging*, pages 207-213, 1999.

D. Barash and D. Comaniciu. A common framework for nonlinear diffusion, adaptive smoothing, bilateral filtering and mean shift. *Image and Video Computing*, 22(1): 73-81, 2004.

C. Bazan and P. Blomgren. Image smoothing and edge detection by nonlinear diffusion and bilateral filter. Research Report CSRCR 200721, San Diego State University, San Diego, California, 2007.

B. Benhamouda. Parameter adaptation for nonlinear diffusion in image processing. Master's thesis, University of Kaiserslautern, Kaiserslautern, Germany, 1994.

E.P. Bennet and L. McMillan. Video enhancement using per-pixel virtual exposures. *ACM Transactions on Graphics*, 24(3):845-852, 2005.

J. Bigün and G.H. Granlund. Optimal orientation detection of linear symmetry. In *Proceedings of First International Conference on Computer Vision*, pages 433-438, London, England, 1987. IEEE Computer Society Press.

T. Brox and J. Weickert. Nonlinear matrix diffusion for optic flow estimation. In L. van Gool, editor, *Lecture Notes in Computer Science*, pages 446-453. Springer-Verlag, Berlin, Germany, 2002.

T. Brox, J. Weickert, B. Burgeth, and P. Mrázek. Nonlinear structure tensors. Technical Report 113, Universität des Saarlandes, Saarbrücken, Germany, 2004.

T. Brox, R. van den Boomgaard, F. Lauze, J. van de Weijer, J. Weickert, P. Mrázek, and P. Kornprobst. Adaptive structure tensors and their applications. Technical Report 141, Universität des Saarlandes, Saarbrücken, Germany, 2005.

T. Brox, J. Weickert, B. Burgeth, and P. Mrázek. Nonlinear structure tensors. *Image and Vision Computing*, 24(1):41-55, 2006.

A. Buades, B. Coll, and J.M. Morel. Neighborhood filters and PDE's. *Numerische Mathematik*, 105(1):1-34, 2006.

A. Canny. A computational approach to edge detection. *IEEE Transactions on Pattern Analysis and Machine Intelligence*, 8(6):679-698, 1986.

F. Catté, P.-L. Lions, J.-M. Morel, and T. Coll. Image selective smoothing and edge detection by nonlinear diffusion. *SIAM Journal of Numerical Analysis*, 29(1):182-193, 1992.

T.F. Chan and L.A. Vese. Active contours without edges. *IEEE Transactions on Image Processing*, 10(2):266-277, 2001.

G.-H. Cottet and L. Germain. Image processing through reaction combined with nonlinear diffusion. *Mathematics of Computation*, 61(204):659-673, 1993.

E. Eisemann and F. Durand. Flash photography enhancement via intrinsic relighting. *ACM Transactions on Graphics*, 23(3):673-678, 2004.

J.J. Fernández and S. Li. An improved algorithm for anisotropic nonlinear diffusion

for denoising cryo-tomograms. *Journal of Structural Biology*, 144(1/2):152-161, 2003.

J.J. Fernández and S. Li. Anisotropic nonlinear filtering of cellular structures in cryo-electron tomography. *Computing in Science and Engineering*, 7(5):54-61, 2005.

W. Förstner and E. Gülch. A fast operator for detection and precise location of distinct points, corners and centres of circular features. In *Proceedings of ISPRS Intercommission Conference on Fast Processing of Photogrammetric Data*, pages 281-305, 1987.

A.S. Frangakis and R. Hegerl. Noise reduction in electron tomographic reconstruction using nonlinear anisotropic diffusion. *Journal of Structural Biology*, 135(3):239-250, 2001.

A.S. Frangakis and R. Hegerl. Nonlinear anisotropic diffusion in three-dimensional electron microscopy. In G.G. Leeuwen and van Hartmanis J., editors, *Lecture Notes in Computer Science*, volume 1682, pages 386-397. Springer Verlag, Berlin, Germany, 1999.

A.S. Frangakis, A. Stoschek, and R. Hegerl. Wavelet transform filtering and nonlinear anisotropic diffusion assessed for signal reconstruction performance on multidimensional biomedical data. *IEEE Transactions on Biomedical Engineering*, 48(2): 213-222, 2001.

S. Frank, B. Gaume, E. Bergmann-Leitner, W. Leitner, E. Robert, F. Catez, C. Smith, and R. Youle. The role of dynamin-related protein 1, a mediator of mitochondrial fission, in apoptosis. *Developmental Cell*, 1(4):515-525, 2001.

T.G. Frey, C.W. Renken, and G.A. Perkins. Insight into mitochondrial structure and function from electron tomography. *Biochimica et Biophysica Acta*, 1555(13): 196-203, 2002.

T.G. Frey, G.A. Perkins, and M.H. Ellisman. Electron tomography of membrane-bound cellular organelles. *The Annual Review of Biophysics and Biomolecular*

Structure, 35:199-224, 2006.

J. Fröhlich and J. Weickert. Image processing using a wavelet algorithm for nonlinear diffusion. Report 104, Laboratory of Technomathematics, University of Kaiserslautern, Kaiserslautern, Germany, 1994.

D.R. Green and J.C. Reed. Mitochondria and apoptosis. *Science*, 281(5381):1309-1312, 1998.

R. Henderson. Realizing the potential of electron cryo-microscopy. *Quarterly Reviews of Biophysics*, 37(1):3-13, 2004.

W. Jiang, M.L. Baker, Q. Wu, C. Bajaj, and W. Chiu. Applications of a bilateral denoising filter in biological electron microscopy. *Journal of Structural Biology*, 144 (1/2):114-122, 2003.

S. Kichenassamy. The Perona-Malik paradox. *SIAM Journal of Applied Mathematics*, 57(5):1328-1342, 1997.

J.R. Kremer, D.N. Mastronarde, and J.R. McIntosh. Computer visualization of three-dimensional image data using IMOD. *Journal of Structural Biology*, 116(1):71-76, 1996.

M. Kuwahara, K. Hachimura, S. Eiho, and M. Kinoshita. Processing of riangio-cardiographic images. In K. Preston and M. Onoe, editors, *Digital Processing of Biomedical Images*, pages 187-202. Plenum Press, New York, New York, 1976.

C. Li, C. Xu, C. Gui, and M.D. Fox. Level set evolution without re-initialization: A new variational formulation. In *Proceedings of IEEE International Conference on Computer Vision and Pattern Recognition*, pages 430-436, 2005.

R. Malladi, J.A. Sethian, and B.C. Vemuri. A fast level set based algorithm for topology-independent shape modeling. *Journal of Mathematical Imaging and Vision*, 6(2/3):269-289, 1996.

S. Marco, T. Bouldier, C. Messaoudi, and J.-L. Rigaud. Electron tomography of biological samples. *Biochemistry*, 69(11):1219-1225, 2004.

T. Meier, K.N. Ngan, and G. Crebbin. A robust markovian segmentation based on highest confidence first. In *Proceedings of IEEE International Conference on Image Processing*, volume 1, pages 216-219. IEEE, 1997.

M. Middendorf and H.-H Nagel. Estimation and interpretation of discontinuities in optical flow fields. In *Proceedings of IEEE Eighth International Conference on Computer Vision*, pages 178-183, Vancouver, Canada, July 2001. IEEE Computer Society Press.

M. Middendorf and H.-H. Nagel. Empirically convergent adaptive estimation of gray-value structure tensors. *Lecture Notes in Computer Science*, 2449:66-74, 2002.

P. Mrázek. *Nonlinear Diffusion for Image Filtering and Monotonicity Enhancement*. PhD thesis, Czech Technical University, Prague, Czech Republic, 2001.

P. Mrázek, J. Weickert, and A. Bruhn. *On Robust Estimation and Smoothing with Spatial and Tonal Kernels*, pages 335-352. Geometric Properties from Incomplete Data. Springer, Dordrecht, Holland, 2006.

A. Munnich and P. Rustin. Clinical spectrum and diagnosis of mitochondrial disorders. *American Journal of Medical Genetics*, 106:4-17, 2001.

M. Nagao and T. Matsuyama. Edge preserving smoothing. *Computer Graphics and Image Processing*, 9(4):394-407, 1979.

H.-H. Nagel and A. Gehrke. Spatiotemporally adaptive estimation and segmentation of OF-fields. *Lecture Notes in Computer Science*, (1407):86-102, 1998.

M. Nitzberg and T. Shiota. Nonlinear image filtering with edge and corner enhancement. *IEEE Transactions on Pattern Analysis and Machine Intelligence*, 14(8): 826-833, 1992.

M. Obeid, A. Tesniere, F. Ghiringhelli, G.M. Fimia, L. Apetoh, J.L. Perfettini, M. Castedo, G. Mignot, T. Panaretakis, N. Casares, D. Metivier, N. Larochette, P. van Endert, F. Ciccosanti, M. Piacentini, L. Zitvogel, and G. Kroemer. Calreticulin exposure dictates the immunogenicity of cancer cell death. *Nature Medicine*,

13(1):54-61, 2007.

S. Osher and R. Fedkiw. *Level Set Methods and Dynamic Implicit Surfaces*, volume 153. Springer, New York, New York, 2003.

S. Osher and J. Sethian. Fronts propagating with curvature-dependent speed: Algorithms based on the hamilton-jacobi formulation. *Journal of Computational Physics*, 79:12-49, 1988.

S. Paris and F. Durand. A fast approximation of the bilateral filter using a signal processing approach. In *Proceedings of European Conference on Computer Vision*, pages 568-580, 2006.

G. Perkins and T. Frey. Electron tomography. In T. Creighton, editor, *Encyclopedia of Molecular Biology*, pages 796-. John Wiley & Sons, New York, New York, 1999.

G.A. Perkins, C.W. Renken, J.Y. Song, T.G. Frey, S.J. Young, S. Lamont, M.E. Martone, S. Lindsey, and M.H. Ellisman. Electron tomography of large, multicomponent biological structures. *Journal of Structural Biology*, 120(3):219-227, 1997.

P. Perona and J. Malik. Scale space and edge detection using anisotropic diffusion. *IEEE Transactions on Pattern Analysis and Machine Intelligence*, 12(7):629-639, 1990.

G. Petschnigg, M. Agrawala, H. Hoppe, R. Szeliski, M. Cohen, and K. Toyama. Digital photography with flash and non-flash image pairs. *ACM Transactions on Graphics*, 23(3):664-672, 2004.

L.A. Pon and E.A. Schon. Preface. In L.A. Pon and E.A. Schon, editors, *Mitochondria*, pages xxiii-xxiv. Academic Press, San Diego, California, 2007.

R. Ramanath and W.E. Snyder. Adapting demosaicking. *Journal of Electronic Imaging*, 12(4):633-642, 2003.

J. A. Sethian. *Level Set Methods and Fast Marching Methods*. Cambridge University Press, Cambridge, Massachusetts, 1999.

S.M. Smith and J.M. Brady. SUSAN-a new approach to low level image processing.

International Journal of Computer Vision, 23(1):45-78, 1997.

B. Tandler, M. Dunlap, C.L. Hoppel, and M. Hassan. Giant mitochondria in a car-diomyopathic heart. *Ultrastructural Pathology*, 26:177-183, 2002.

C. Tomasi and R. Manduchi. Bilateral filtering for gray and color images. In *Proceedings of IEEE International Conference on Computer Vision*, pages 839-846. IEEE, 1998.

R. van den Boomgaard. The kuwahara-nagao operator decomposed in terms of a linear smoothing and a morphological sharpening. In H. Talbot and R. Beare, editors, *Proceedings of 6th International Symposium on Mathematical Morphology*, pages 283-292, Sydney, Australia, April 2002. CSIRO Publishing.

R. van den Boomgaard and J. van de Weijer. Robust estimation of orientation for texture analysis. In *Proceedings of Texture 2002, 2nd International Workshop on Texture Analysis and Synthesis*, Copenhagen, Denmark, June 2002.

N. Volkmann. A novel three-dimensional variant of the watershed transform for segmentation of electron density maps. *Journal of Structural Biology*, 138(12): 123-129, 2002.

J. Weickert. Efficient image segmentation using partial differential equations and morphology. *Pattern Recognition*, 34(9):1813-1824, 2001.

J. Weickert. Theoretical foundations of anisotropic diffusion in image processing. In *Proceedings of 7th TFCV on Theoretical Foundations of Computer Vision*, volume 11 of *Computing Supplement*, pages 221-236, London, 1994a. Springer-Verlag.

J. Weickert. Anisotropic diffusion filters for image processing based quality control. In A. Fasano and M. Primicerio, editors, *Proceedings of Seventh European Conference on Mathematics in Industry*, pages 355-362. Teubner, Stuttgart, Germany, 1994b.

J. Weickert. Scale-space properties of nonlinear diffusion filtering with diffusion ten-sor. Report 110, Laboratory of Technomathematics, University of Kaiserslautern, Kaiserslautern, Germany, 1994c.

J. Weickert. Multiscale texture enhancement. In V. Hlaváč and Šára, editors, *Computer Analysis of Images and Patterns, Lecture Notes in Computer Science*, pages 230-237. Springer, Berlin, Germany, 1995.

J. Weickert. Theoretical foundations of anisotropic diffusion in image processing. *Computing Supplement*, 11:221-236, 1996a.

J. Weickert. *Anisotropic Diffusion in Image Processing*. PhD thesis, Universität Kaiserslautern, Kaiserslautern, Germany, 1996b.

J. Weickert. *Anisotropic Diffusion in Image Processing*. ECMI Series. Teubner-Verlag, Stuttgart, 1998.

J. Weickert. Coherence-enhancing diffusion of colour images. *Image and Vision Computing*, 17(3):201-212, 1999a.

J. Weickert. Coherence-enhancing diffusion filtering. *International Journal of Computer Vision*, 31(2/3):111-127, 1999b.

J. Weickert and T. Brox. Diffusion and regularization of vector- and matrix-valued images. In M. Z. Nashed and O. Scherzer, editors, *Inverse Problems, Image Analysis, and Medical Imaging. Contemporary Mathematics*, volume 313, pages 251-268. AMS, Providence, Rhode Island, 2002.

J. Weickert and C. Schnörr. PDE-based preprocessing of medical images. *Kunstliche Intelligenz*, 3:5-10, 2000.

J. Weickert, B.M.t.H. Romeny, and M.A. Viergever. Efficient and reliable schemes for nonlinear diffusion filtering. *IEEE Transactions on Image Processing*, 7(3):398-410, 1998.

R.T. Whitaker and S.M. Pizer. A multi-scale approach to non-uniform diffusion. *Computer Vision, Graphics, and Image Processing: Image Understanding*, 57(1): 99-110, 1993.

H. Winnermöller, S.C. Olsen, and B. Gooch. Real-time video abstraction. *ACM*

Transactions on Graphics, 25(3):1221-1226, 2006.

N. Zamzami, C. Maisse, D. Métivier, and G. Kroemer. Measurement of membrane permeability and the permeability transition of mitochondria. In L.A. Pon and E.A. Schon, editors, *Mitochondria*, volume 80 of *Methods in Cell Biology*, chapter 16, pages 327-340. Academic Press, San Diego, California, 2007.